© 2015. Published by The Company of Biologists Ltd | Development (2015) 142, 840-845 doi:10.1242/dev.116657

RESEARCH REPORT

STEM CELLS AND REGENERATION

Striatal astrocytes produce neuroblasts in an excitotoxic model of Huntington's disease

Giulia Nato[1,2], Alessia Caramello[1,2], Sara Trova[1,2], Valeria Avataneo[1,2], Chiara Rolando[3], Verdon Taylor[3], Annalisa Buffo[2,4], Paolo Peretto[1,2,*,‡] and Federico Luzzati[1,2,*,‡]

ABSTRACT

In the adult brain, subsets of astrocytic cells residing in well-defined neurogenic niches constitutively generate neurons throughout life. Brain lesions can stimulate neurogenesis in otherwise non-neurogenic regions, but whether local astrocytic cells generate neurons in these conditions is unresolved. Here, through genetic and viral lineage tracing in mice, we demonstrate that striatal astrocytes become neurogenic following an acute excitotoxic lesion. Similar to astrocytes of adult germinal niches, these activated parenchymal progenitors express nestin and generate neurons through the formation of transit amplifying progenitors. These results shed new light on the neurogenic potential of the adult brain parenchyma.

KEY WORDS: Neural stem cells, Parenchymal progenitors, Stem cell quiescence, Lesion-induced neurogenesis, Huntington's disease, Mouse

INTRODUCTION

In adult neurogenic niches, astrocytic cells produce neurons throughout life (Fuentealba et al., 2012). Parenchymal astrocytes can become neurogenic *in vitro* when isolated from the lesioned neocortex (Buffo et al., 2008; Sirko et al., 2013) or *in vivo* after overexpression of specific transcription factors (Niu et al., 2013). However, whether parenchymal astrocytes can spontaneously generate neurons *in vivo* is unclear (Dimou and Götz, 2014). The adult brain parenchyma has been generally considered gliogenic and not permissive for the activity of neuronal progenitors (Lim et al., 2000; Ninkovic and Götz, 2013; Shihabuddin et al., 2000). Nonetheless, examples of parenchymal neurogenesis are emerging (Bi et al., 2011; Luzzati et al., 2006, 2011b; Ohira et al., 2010). For instance, we previously demonstrated that clusters of proliferating cells with features of transient amplifying progenitors (TAPs) produce neurons in the striatum of rabbits (Luzzati et al., 2006) and in a mouse model of striatal degeneration (Luzzati et al., 2011b).

Here, we analysed striatal neurogenesis in the quinolinic acid (QA) lesion mouse model of Huntington's disease (Fan and Raymond, 2007). We show that such a lesion activates striatal astrocytes to produce neurons.

RESULTS AND DISCUSSION

At 5 weeks post-QA lesion (w.p.l.), numerous DCX^+ neuroblasts were present in the striatum and organised into clusters or as individual cells (Fig. 1A-E). As in other models of striatal neurogenesis (Liu et al., 2009; Luzzati et al., 2011b), these neuroblasts expressed SP8, a transcription factor typical of lateral/caudal ganglionic eminence-derived interneurons (Ma et al., 2012; Waclaw et al., 2006), and some of them expressed NeuN (RBFOX3 – Mouse Genome Informatics; data not shown) and attained complex morphologies (supplementary material Fig. S1). The clusters of DCX^+ cells were closely associated to clusters of cells expressing the proliferation marker Ki67 (MKI67 – Mouse Genome Informatics), with numerous cells colabelled for DCX (Fig. 1B,C,E).

Based on clustering and the differential expression of Ki67 and DCX we could define four striatal cell types that were induced by QA: clustered $Ki67^+/DCX^-$ cells (cK), clustered $Ki67^+/DCX^+$ cells (cKD), clustered $DCX^+/Ki67^-$ cells (cD) and individual $DCX^+/Ki67^-$ cells (iD) (Fig. 1C-F). The cK, cKD and cD cells appeared between 2 and 3 w.p.l. (2 versus 3 w.p.l., Tukey's post-hoc test: cK, P=0.010; cKD, P=0.005; cD, P=0.021; Fig. 1F) and, although their number remained constant after 3 weeks (ANOVA: cK, $F_{2,7}$=2.464, P=0.155; cKD, $F_{2,7}$=0.383, P=0.695; cD, $F_{2,7}$=0.419, P=0.673), at all time points a high proportion incorporated BrdU when injected 4 days before sacrifice (supplementary material Fig. S2A,D). This indicates that cK, cKD and cD cells have a high turnover rate. By contrast, iD cells showed a delayed increase that peaked at 4 w.p.l. (Tukey's post-hoc test: 2 versus 3 weeks, P=0.226; 3 versus 4 weeks, P=0.001; Fig. 1F) accompanied by a reduction in the fraction of $BrdU^+$ cells over time (Tukey's post-hoc test: 3 versus 4 weeks, P=0.031; supplementary material Fig. S2C,D). Thus, this latter population appears later and has a lower turnover rate.

Interestingly, most cK cells expressed the TAP markers ASCL1 (Parras et al., 2004) and SOX9 (Cheng et al., 2009) (Fig. 1G-I; data not shown). Collectively, these data suggest that, as proposed in other models of striatal neurogenesis (Luzzati et al., 2006, 2011b), QA stimulates the appearance of TAP-like progenitors (cK cells) that give rise to neuroblasts that initially cluster (cKD, cD cells) and subsequently disperse as individual cells (iD cells). At 6 months after QA, striatal TAPs and neuroblasts were still present and could incorporate BrdU (supplementary material Fig. S3), suggesting that QA results in the long-term establishment of an intrastriatal neurogenic niche.

The induction of neurogenic potential in resident parenchymal cells was further supported by the appearance of self-renewing multipotent neurospherogenic cells in the striatum at 5 w.p.l. (supplementary material Fig. S4; data not shown). Interestingly, clusters of cK, cKD and cD cells were generally closely associated to $GFAP^+$ astrocytes, which were occasionally proliferating, as assessed through both Ki67 and BrdU (supplementary material Fig. S5). Using hGFAP-GFP mice (Platel et al., 2009; Zhuo et al., 1997) we could establish that $GFP^+/Ki67^+$ proliferating astrocytes represented 8±3% of all cK cells at 5 w.p.l. (Fig. 1I-L). These observations support the contention that cK cells and their progeny originate from striatal astrocytes.

[1]Department of Life Sciences and Systems Biology (DBIOS), University of Turin, Turin 10123, Italy. [2]Neuroscience Institute Cavalieri Ottolenghi (NICO), Orbassano 10043, Italy. [3]Departement of Biomedecin, University of Basel, Basel 4050, Switzerland. [4]Department of Neuroscience Rita Levi-Montalcini, University of Turin, Turin 10126, Italy.

*These authors contributed equally to this work

‡Authors for correspondence (paolo.peretto@unito.it; federico.luzzati@unito.it)

Received 14 August 2014; Accepted 14 January 2015

Development (2015) 142, 840-845 doi:10.1242/dev.116657

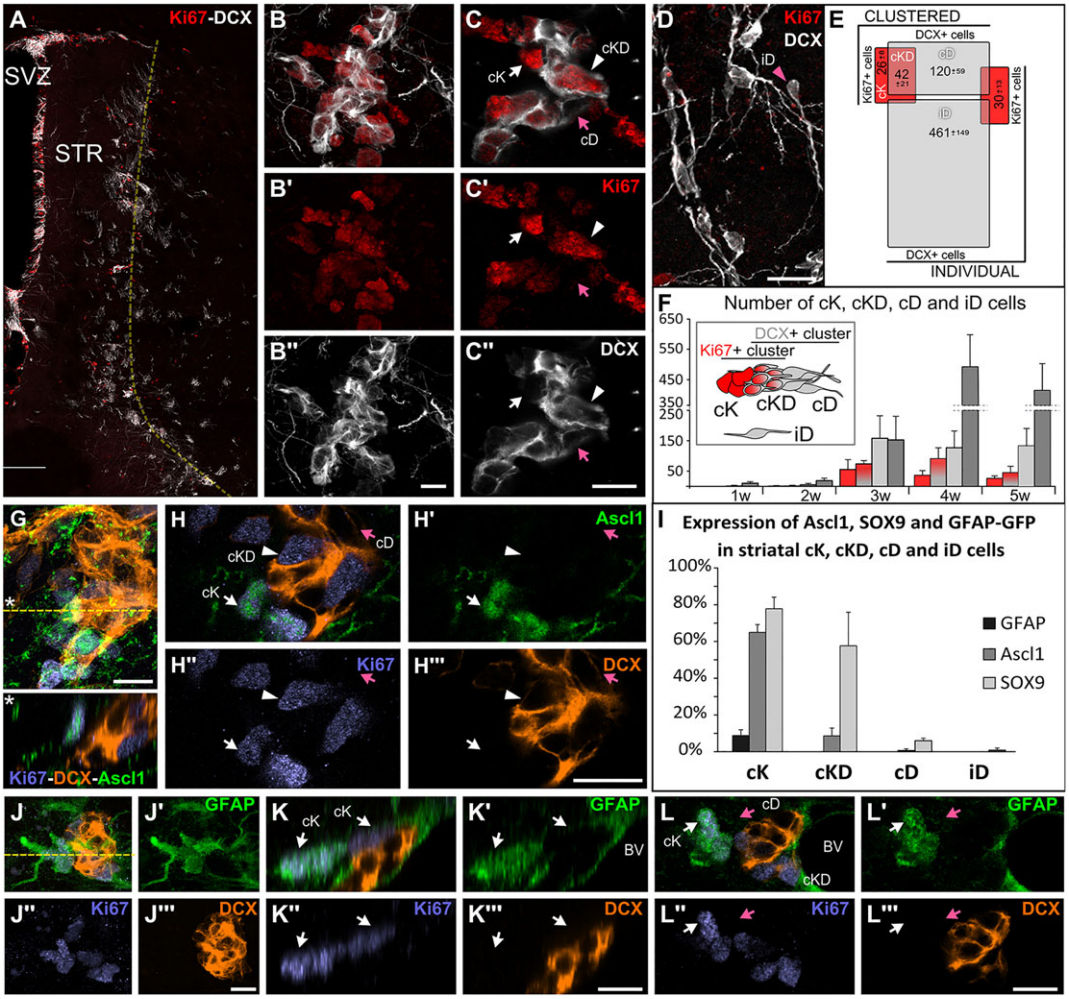

Fig. 1. Ki67$^+$ and DCX$^+$ cells in the 5 w.p.l. striatum. (A) Coronal section showing striatal Ki67$^+$ (red) and DCX$^+$ (white) cells densely packed at the lesion border (yellow dashed line). (B-C″) *z*-projection (B-B″) and single confocal plane (C-C″) of a Ki67$^+$ cluster partially overlapping with a DCX$^+$ cluster. (D) iD cells. (E) Each square represents the number of individual (bottom right) or clustered (top left) DCX$^+$ (grey) and Ki67$^+$ (red) cells in the striatum at 5 w.p.l. The overlap of these populations is in dark red. (F) Number of cK, cKD, cD and iD cells in the striatum at 1, 2, 3, 4 and 5 w.p.l. A schematic view of the cell types is shown in the inset. (G-H‴) *z*-projection (G), reslice (asterisk in G marks plane of section beneath) and single confocal plane (H-H‴) of a Ki67$^+$ (violet) and DCX$^+$ (orange) cluster immunolabelled for ASCL1 (green). (I) Percentage of cK, cKD, cD and iD cells expressing GFAP-GFP, ASCL1 and SOX9. (J-L‴) *z*-projection (J-J‴), reslice (K-K‴, at yellow dashed line in J) and single confocal plane (L-L‴) of a Ki67$^+$ (violet) and DCX$^+$ (orange) cluster showing cK cells labelled for GFAP-GFP (green). Error bars indicate s.d. Scale bars: 200 µm in A; 10 µm in B-C″,G-H‴; 20 µm in D 10 µl in J-L‴.

To explore this possibility further, we first performed cell fate-mapping analysis using transgenic mice expressing the tamoxifen-inducible recombinase CreER^{T2} under the control of diverse cell type-specific promoters, namely *Glast* (*Slc1a3* – Mouse Genome Informatics), nestin (*Nes*) and *Ng2* (*Cspg4* – Mouse Genome Informatics). GLAST is a pan-astrocytic marker (Dimou and Götz, 2014), whereas nestin more specifically associates with active neurogenic astrocytes (Codega et al., 2014) and some oligodendrocyte progenitors (Boda et al., 2015), while NG2 is specifically expressed by oligodendrocyte progenitors (Zhu et al., 2011). Accordingly, in intact animals 1 week after tamoxifen, recombined YFP$^+$ cells represented 44±3% of all S100b$^+$ striatal astrocytes in GLAST-CreER^{T2} mice and 10±6% in Nestin-CreER^{T2} animals. In the NG2-CreER^{T2} line, astrocytes were not targeted (supplementary material Fig. S6).

To determine whether cells expressing these genes are the source of intrastriatal TAPs and neuroblasts after lesion, tamoxifen was administered 1 week before QA (bQA). In addition, for each genotype a second group of animals was treated with tamoxifen at 4 w.p.l. (aQA) to identify possible injury-related changes in the phenotype of the neurogenic progenitors after their activation. In all cases animals were analysed at 5 w.p.l. (Fig. 2A). In NG2-CreER^{T2} animals, we never observed DCX$^+$ neuroblasts expressing the reporter YFP, either in the striatum or in the subventricular zone-olfactory bulb (SVZ-OB) system (data not shown), indicating that NG2$^+$ cells are not neurogenic in our model. By contrast, in the SVZ of GLAST-CreER^{T2} and Nestin-CreER^{T2} animals, YFP$^+$ cells included putative TAPs (Ki67$^+$/DCX$^-$), proliferating (DCX$^+$/Ki67$^+$) and postmitotic (DCX$^+$/Ki67$^-$) neuroblasts (Fig. 2A-C). The percentage of YFP$^+$ cells did not differ between strains (supplementary material Table S1), indicating similar efficiency of nestin- or GLAST-driven recombination in SVZ neurogenic astrocytes.

In the striatum of GLAST-CreER^{T2} bQA and aQA animals, YFP was expressed by cK, cKD, cD and iD cells, indicating that these cells originate from astrocytes that express GLAST both before and after the QA lesion (Fig. 2A,D,E; supplementary material Fig. S7A,B). YFP$^+$ postmitotic neuroblasts (cD and iD) were less numerous in the

Development (2015) 142, 840-845 doi:10.1242/dev.116657

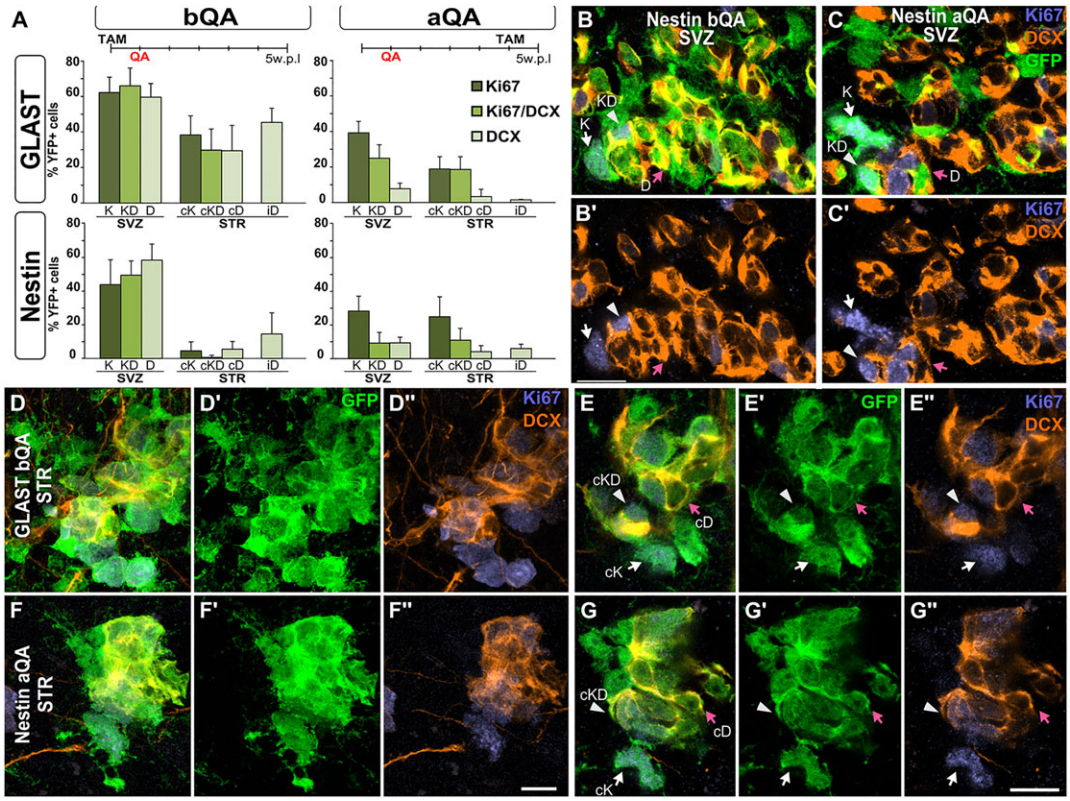

Fig. 2. Genetic lineage tracing. (A) Fraction of SVZ and striatal (STR) putative TAP cells (Ki67$^+$; K, cK), proliferating (Ki67$^+$/DCX$^+$; KD, cKD) and post-mitotic (DCX$^+$; D, cD, iD) neuroblasts that expressed YFP in 5 w.p.l. GLAST-CreER^{T2} (top row) and Nestin-CreER^{T2} (bottom row) animals that received TAM before (bQA, left column) or after (aQA, right column) lesion. Error bars indicate s.d. (B-C′) Single confocal plane of the SVZ of a Nestin-CreER^{T2} bQA (B) and aQA (C) labelled for Ki67 (violet), DCX (orange) and GFP (green). (D-G″) *z*-projections (D,F) and single confocal planes (E,G) of recombined Ki67$^+$/DCX$^+$ clusters. Scale bars: 10 µm.

striatum of GLAST-CreER^{T2} aQA animals, but increased to levels comparable to those of YFP$^+$ proliferative cells (cK and cKD) in the GLAST-CreER^{T2} bQA animals (Fig. 2A; supplementary material Table S1A), further supporting that cK and cKD cells are early stages of the striatal neurogenic lineage. Three-dimensional reconstructions in GLAST-CreER^{T2} bQA animals indicated that the morphology of the GFP$^+$ iD cells was comparable to that of their GFP$^-$ counterparts (supplementary material Fig. S8). Thus, GLAST$^+$ astrocytes are the source of QA-induced intrastriatal TAPs and neuroblasts.

In Nestin-CreER^{T2} bQA mice, YFP$^+$ cells corresponding to the striatal cell types (cK, cKD, cD and iD) were very rare (Fig. 2A). However, in Nestin-CreER^{T2} aQA animals, the levels of genetic labelling of cK and cKD cells were greatly increased and reached similar levels to those seen in GLAST-CreER^{T2} aQA animals (Fig. 2A,F,G; supplementary material Table S1C). Interestingly, although nestin was mostly absent from striatal astrocytes under normal conditions, several YFP$^+$ cells with astrocytic morphology appeared in Nestin-CreER^{T2} aQA animals (supplementary material Fig. S7C,D). These findings suggest that the resident GLAST$^+$ striatal astrocytes upregulate the expression of nestin after lesion and generate cK, cKD, cD and iD cells.

To directly confirm both the striatal origin of the neurogenic progenitors and their astrocytic identity, we performed intrastriatal injections of either a GFP-tagged lentiviral vector (VSVG-GFP; n=3) or an adenoviral vector carrying Cre recombinase under the control of the mouse *Gfap* promoter (Ad:GFAP-Cre; n=3; Merkle et al., 2007) 1 week before QA lesion. Whereas VSVG-GFP showed broad cellular tropism (data not shown), injection of Ad:GFAP-Cre into the striatum of R26R reporter mice resulted in the expression of YFP almost exclusively in astrocytes (supplementary material Fig. S9). Only animals with no YFP staining in the SVZ-OB system were analysed. In both cases, at 5 w.p.l. serial section 3D reconstructions of the whole striatum revealed multiple examples of YFP$^+$ or GFP$^+$ cK, cKD, cD and iD cells (Figs 3 and 4). The morphology of these latter cells was consistent with that of GFP$^-$ iD cells (Fig. 4B-E). These data indicate that striatal astrocytes generate TAPs and neuroblasts after lesion.

Notably, in both our genetic and viral fate-mapping analyses about 85% of the striatal Ki67$^+$ clusters exhibiting reporter expression were entirely composed of cells expressing YFP or GFP (Fig. 2D-G, Fig. 3C,D and Fig. 4F,G; see Materials and Methods for details), indicating that proliferative clusters originate mostly from the clonal expansion of a single striatal astrocytic progenitor.

SVZ progenitors have been shown to generate neuroblasts for the lesioned striatum (Liu et al., 2009). To examine whether these progenitors can further contribute to the intrastriatal TAPs, we injected Ad:GFAP-Cre or a TAT-Cre to respectively target the dorsolateral and the periventricular SVZ of R26R mice 1 week before QA. In the striatum of these animals at 5 w.p.l. we observed only a few iD cells expressing YFP (supplementary material Fig. S10), suggesting that striatal TAPs originate only from local astrocytes.

Taken together, these results indicate that some striatal astrocytes are quiescent neuronal progenitors that become activated after QA lesion. Like neurogenic astrocytes of other neurogenic niches, these cells upregulate nestin in their active state (Codega et al., 2014) and

Development (2015) 142, 840-845 doi:10.1242/dev.116657

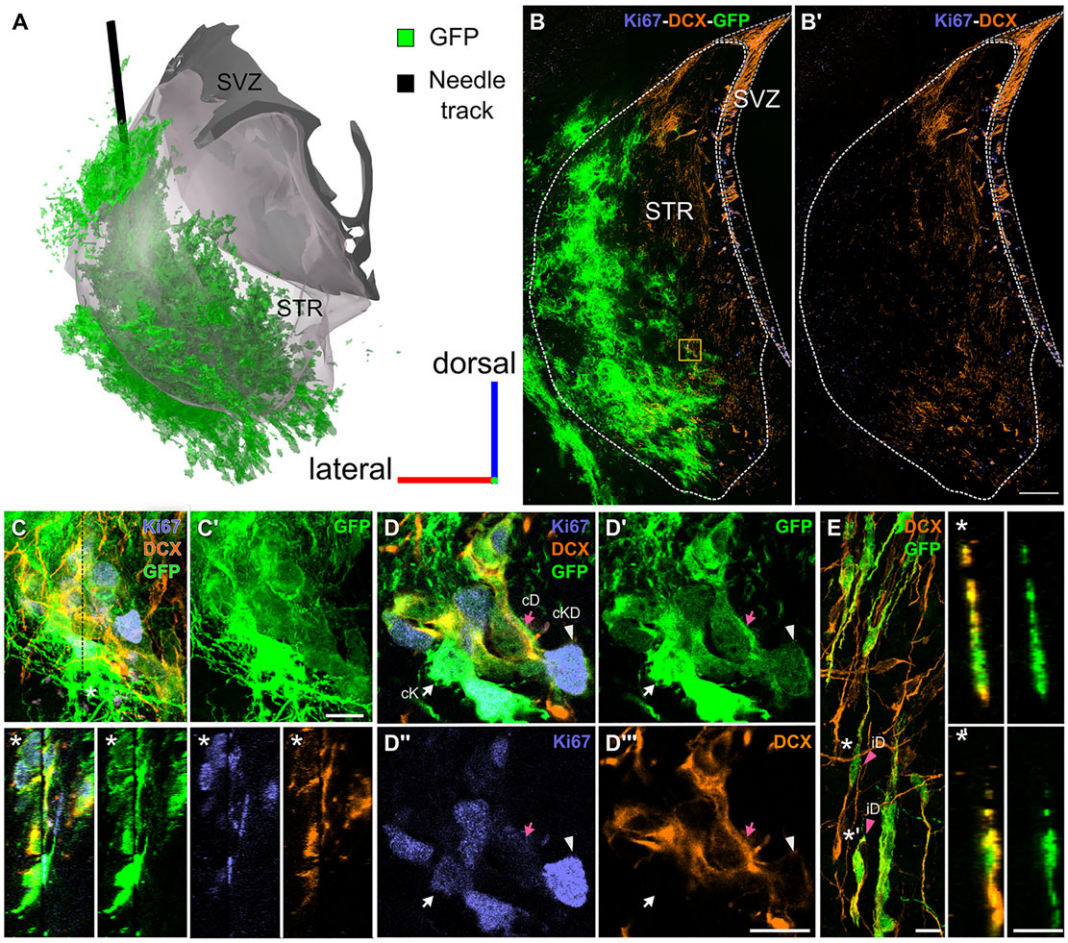

Fig. 3. Viral lineage tracing. (A) 3D reconstruction of SVZ (grey), striatum (transparent grey) and GFP staining (green) of a 5 w.p.l. animal injected with VSVG-GFP 1 week before QA. (B,B′) Coronal section at the level of the injection site labelled for DCX (orange), Ki67 (white) and GFP (green). (C-D‴) *z*-projection (C), reslice (asterisk, at black dotted line) and single confocal plane (D-D‴) of a cluster (box in B) made by cK, cKD and cD cells reconstructed from two successive 50 µm serial sections. (E) *z*-projection and reslices (asterisk and asterisk with prime) of GFP$^+$ iD cells. Scale bars: 200 µm in B,B′; 10 µm in C-E.

produce neurons through ASCL1$^+$ and SOX9$^+$ TAPs (Dimou and Götz, 2014; Fuentealba et al., 2012). However, striatal progenitors and/or their microenvironment may possess unique features that enable them to produce neurons in the brain parenchyma. Unravelling these features might help to unleash the full neurogenic potential of the adult brain, a fundamental prerequisite in order to design cell replacement therapies for brain repair. Interestingly, while this study was under revision the activation of neurogenic potential in striatal astrocytes was also demonstrated in a model of stroke (Magnusson et al., 2014) and under physiological conditions during guinea pig development (Luzzati et al., 2014). Thus, in contrast to SVZ and dentate gyrus neuronal progenitors, which are constitutively active, other populations of neurogenic astrocytes are activated only under specific conditions. The fate potential of these progenitors remains an important issue. Most neuroblasts generated in both the normal and lesioned striatum have a short life-span, but attain complex and specific morphologies (Luzzati et al., 2011a,b, 2014). These transient neurons might sustain a new type of adult brain plasticity that merits further exploration.

MATERIALS AND METHODS

Animals

All animal experiments were approved by the Italian Ministry of Health and the Bioethical Committee of the University of Turin. Experiments were performed on 8- to 12-week animals. C57BL/6 lesioned mice received two intraperitoneal injections (6 h apart) of 5-bromo-2-deoxyuridine (BrdU, Sigma-Aldrich; 50 mg/kg in 0.1 M Tris pH 7.4) 4 days before sacrifice. Tamoxifen (TAM, Sigma-Aldrich T5648-1G) was dissolved in corn oil (Sigma-Aldrich C8267) and 2.5 mg was administered by forced feeding (oral gavage) twice with a 24 h interval.

Histology

Animals were anesthetised with a ketamine (100 mg/kg ketavet, Gellini) and xylazine (33 mg/kg rompun, Bayer) solution and perfused with a solution of 4% paraformaldehyde (PFA) and 2% picric acid (AnalytiCals, Carlo Erba 409302) in 0.1 M sodium phosphate buffer (PB) pH 7.4. Brains were then post-fixed for 3 h, cryoprotected in 30% sucrose (Fluka 84100) in 0.1 M PB pH 7.4, embedded at −80°C in Killik/OCT (Bio-Optica 05-9801), and cryostat sectioned in a series of 50 µm-thick sections.

Generation of viral vectors and TAT-Cre

VSVG-GFP vector stocks were produced by transient transfection of the transfer plasmid expressing eGFP under the control of the CMV promoter, the packaging plasmids pMDLg/pRRE and pRSV.REV, and the VSV envelope plasmid pMD2.VSV-G in HEK293T cells as described (Follenzi et al., 2000). Viral particles were purified and concentrated by ultracentrifugation as described (Dull et al., 1998). Vector titre on HeLa cells was 2×10^9 TU/ml. The virus was then diluted 1/20 in PBS containing 0.6% glucose and frozen.

Generation of Ad:GFAP-Cre virus was described previously (Merkle et al., 2014). Briefly, HEK293 cells were infected to produce replication-defective adenovirus, which was purified using the Fast-Trap

Development (2015) 142, 840-845 doi:10.1242/dev.116657

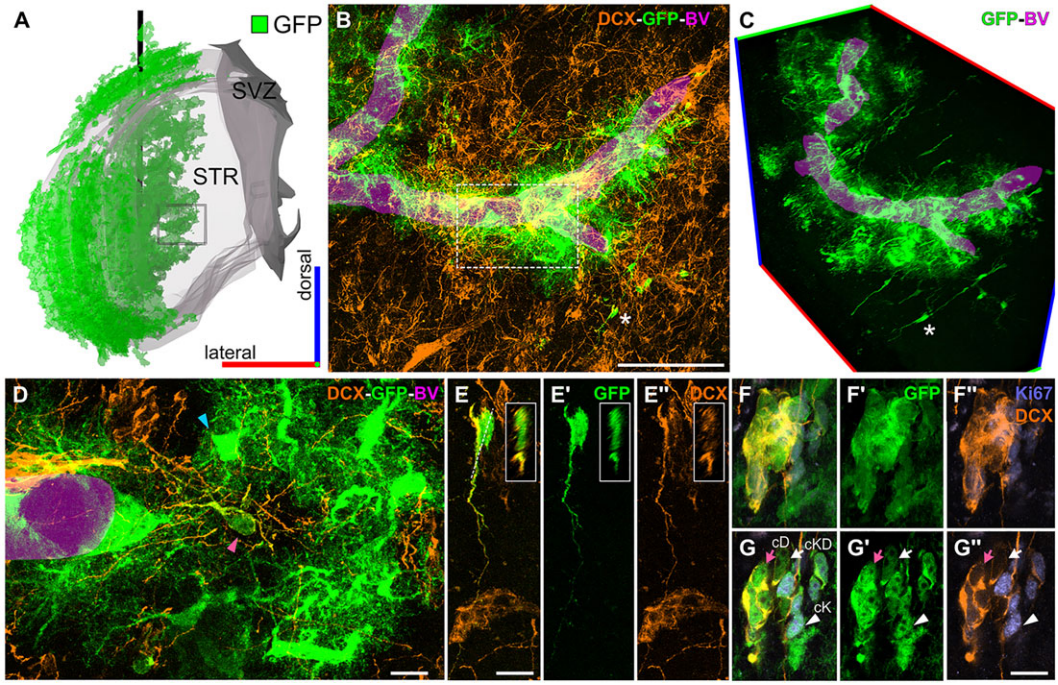

Fig. 4. Intrastriatal injection of Ad:GFAP-Cre. (A) 3D reconstruction of SVZ (grey), striatum (transparent grey), GFP staining (green) and needle track (black bar) of a 5 w.p.l. R26R-YFP animal injected with Ad:GFAP-Cre 1 week before QA. (B,C) *z*-projection (B) and perspective view (C) of a 3D reconstruction comprising four 50 µm-thick sections labelled with YFP (green) and DCX (orange) (box in A). Most YFP^+ cells are distributed around blood vessels (BV, magenta). However, some DCX^+ cells are also found deeper in the striatal parenchyma. (D) *z*-projection of a single 50 µm section (box in B) showing YFP^+/DCX^+ (pink arrowhead) and YFP^+/DCX^- (blue arrowhead) cells near a blood vessel. (E-E″) Higher magnification of an individual YFP^+/DCX^+ cell, as indicated by the asterisk in B,C. The inset shows a reslice. (F-G″) *z*-projection (F-F″) and single confocal plane (G-G″) of a cluster made by cK, cKD and cD cells. Scale bars: 100 µm in B; 10 µm in D-G″.

Adenovirus Purification and Concentration Kit (Millipore). The titre was 1×10^{10} infectious particles/ml. TAT-Cre recombinant protein was produced as previously described (Peitz et al., 2002).

Stereotaxic injections

Mice were anesthetised with 0.3 ml/kg ketamine and 0.2 ml/kg xylazine, positioned in a stereotaxic apparatus (Stoelting) and injected with a pneumatic pressure injection apparatus (Picospritzer II, General Valve Corporation). Injection coordinates: QA (Sigma-Aldrich P6,320-4; 1 µl diluted to 120 mM in 0.1 M PB), +0.1 mm AP, −2.1 mm ML and −2.6 mm DV; VSVG-GFP and Ad:GFAP-Cre, 0.8 mm AP, −2.1 mm ML and −3.2 mm DV (n=3 for each vector). Ad:GFAP-Cre virions driving Cre recombinase expression in $GFAP^+$ cells were injected into R26YFP reporter mice. For both vectors, we analysed only animals in which the SVZ and OB were entirely free of reporter-positive cells. To target the SVZ, VSVG-GFP and TAT-Cre were injected respectively at +1.2 mm AP, −1 mm ML and −1.3 mm DV and at +3 mm AP, −0.8 mm ML and −2.9 mm DV.

Immunofluorescence

Sections were incubated for 48 h at 4°C in 0.01 M PBS pH 7.4 containing 2% Triton X-100, 1:100 normal donkey serum and primary antibodies (supplementary material Table S2). For BrdU staining, sections were pre-incubated in 2 M HCl for 30 min at 37°C and then rinsed in 0.1 M borate buffer pH 8.5. Sections were incubated overnight with appropriate secondary antibodies (supplementary material Table S2) and coverslipped with antifade mounting medium Mowiol (4-88 reagent, Calbiochem 475904).

Image processing and 3D reconstructions

Images were processed using ImageJ (NIH) and Photoshop 7.0 (Adobe Systems). Confocal microscopy serial section 3D reconstructions were performed as described (Luzzati et al., 2011a). Briefly, images from each section were stitched in Fiji (Preibisch et al., 2009), aligned with Reconstruct 1.1 (Fiala, 2005) or with TracKEM2 (Cardona et al., 2010) and neurons were traced in NeuronStudio (Wearne et al., 2005). 3D models were rendered in Blender 2.6. (Blender Foundation) and Vaa3D (Peng et al., 2014).

Acknowledgements

We thank Claudio Giachino for critical reading of the manuscript; Rosanna Parlato and Ghunther Shutz for the Nestin-CreER^{T2} transgenic line; Arturo Alvarez-Buylla for the Ad:GFAP-Cre plasmids; Elisa Vigna for VSVG-GFP plasmids; and Massimiliano Mazzone for TAT-Cre. This work is dedicated to the memory of Aldo Fasolo.

Competing interests

The authors declare no competing or financial interests.

Author contributions

F.L., P.P. and G.N. designed the experiments. A.B. contributed to the experimental design. F.L. and G.N. performed the experiments and analysed the data. A.C. contributed to the lineage-tracing study. S.T. and V.A. contributed to the stereological analyses. V.T. provided the Ad:GFAP-Cre viral vector. C.R. produced and tested the viral vectors. A.B. contributed to the neurosphere assays. F.L., P.P. and A.B. wrote the paper. V.T. critically commented on the paper.

Funding

This work was supported by Progetti di Ricerca di Interesse Nazionale (PRIN)-Peretto 2010-2011 and partly by PRIN 20107MSMA4 to A.B.

Supplementary material

Supplementary material available online at
http://dev.biologists.org/lookup/suppl/doi:10.1242/dev.116657/-/DC1

References

Bi, B., Salmaso, N., Komitova, M., Simonini, M. V., Silbereis, J., Cheng, E., Kim, J., Luft, S., Ment, L. R., Horvath, T. L. et al. (2011). Cortical glial fibrillary acidic protein-positive cells generate neurons after perinatal hypoxic injury. *J. Neurosci.* **31**, 9205-9221.

Boda, E., Di Maria, S., Rosa, P., Taylor, V., Abbracchio, M. P. and Buffo, A. (2015). Early phenotypic asymmetry of sister oligodendrocyte progenitor cells after mitosis and its modulation by aging and extrinsic factors. *Glia* **63**, 271–286.

Buffo, A., Rite, I., Tripathi, P., Lepier, A., Colak, D., Horn, A.-P., Mori, T. and Gotz, M. (2008). Origin and progeny of reactive gliosis: a source of multipotent cells in the injured brain. *Proc. Natl. Acad. Sci. USA* **105**, 3581-3586.
Cardona, A., Saalfeld, S., Preibisch, S., Schmid, B., Cheng, A., Pulokas, J., Tomancak, P. and Hartenstein, V. (2010). An integrated micro- and macroarchitectural analysis of the Drosophila brain by computer-assisted serial section electron microscopy. *PLoS Biol.* **8**, e1000502.
Cheng, L.-C., Pastrana, E., Tavazoie, M. and Doetsch, F. (2009). miR-124 regulates adult neurogenesis in the subventricular zone stem cell niche. *Nat. Neurosci.* **12**, 399-408.
Codega, P., Silva-Vargas, V., Paul, A., Maldonado-Soto, A. R., Deleo, A. M., Pastrana, E. and Doetsch, F. (2014). Prospective identification and purification of quiescent adult neural stem cells from their in vivo niche. *Neuron* **82**, 545-559.
Corsini, N. S., Sancho-Martinez, I., Laudenklos, S., Glagow, D., Kumar, S., Letellier, E., Koch, P., Teodorczyk, M., Kleber, S., Klussmann, S. et al. (2009). The death receptor CD95 activates adult neural stem cells for working memory formation and brain repair. *Cell Stem Cell* **5**, 178-190.
Dimou, L. and Götz, M. (2014). Glial cells as progenitors and stem cells: new roles in the healthy and diseased brain. *Physiol. Rev.* **94**, 709-737.
Dull, T., Zufferey, R., Kelly, M., Mandel, R. J., Nguyen, M., Trono, D. and Naldini, L. (1998). A third-generation lentivirus vector with a conditional packaging system. *J. Virol.* **72**, 8463-8471.
Fan, M. M. Y. and Raymond, L. A. (2007). N-methyl-D-aspartate (NMDA) receptor function and excitotoxicity in Huntington's disease. *Prog. Neurobiol.* **81**, 272-293.
Fiala, J. C. (2005). Reconstruct: a free editor for serial section microscopy. *J. Microsc.* **218**, 52-61.
Follenzi, A., Ailles, L. E., Bakovic, S., Geuna, M. and Naldini, L. (2000). Gene transfer by lentiviral vectors is limited by nuclear translocation and rescued by HIV-1 pol sequences. *Nat. Genet.* **25**, 217-222.
Fuentealba, L. C., Obernier, K. and Alvarez-Buylla, A. (2012). Adult neural stem cells bridge their niche. *Cell Stem Cell* **10**, 698-708.
Lim, D. A., Tramontin, A. D., Trevejo, J. M., Herrera, D. G., García-Verdugo, J. M. and Alvarez-Buylla, A. (2000). Noggin antagonizes BMP signaling to create a niche for adult neurogenesis. *Neuron* **28**, 713-726.
Liu, X. S., Chopp, M., Zhang, R. L., Hozeska-Solgot, A., Gregg, S. C., Buller, B., Lu, M. and Zhang, Z. G. (2009). Angiopoietin 2 mediates the differentiation and migration of neural progenitor cells in the subventricular zone after stroke. *J. Biol. Chem.* **284**, 22680-22689.
Lowenstein, P. R. and Castro, M. G. (2003). Inflammation and adaptive immune responses to adenoviral vectors injected into the brain: peculiarities, mechanisms, and consequences. *Gene Ther.* **10**, 946-954.
Luzzati, F., De Marchis, S., Fasolo, A. and Peretto, P. (2006). Neurogenesis in the caudate nucleus of the adult rabbit. *J. Neurosci.* **26**, 609-621.
Luzzati, F., Fasolo, A. and Peretto, P. (2011a). Combining confocal laser scanning microscopy with serial section reconstruction in the study of adult neurogenesis. *Front. Neurosci.* **5**, 70.
Luzzati, F., De Marchis, S., Parlato, R., Gribaudo, S., Schütz, G., Fasolo, A. and Peretto, P. (2011b). New striatal neurons in a mouse model of progressive striatal degeneration are generated in both the subventricular zone and the striatal parenchyma. *PLoS ONE* **6**, e25088.
Luzzati, F., Nato, G., Oboti, L., Vigna, E., Rolando, C., Armentano, M., Bonfanti, L., Fasolo, A. and Peretto P. (2014). Quiescent neuronal progenitors are activated in the juvenile guinea pig lateral striatum and give rise to transient neurons. *Development* **141**, 4065-4075.
Ma, T., Zhang, Q., Cai, Y., You, Y., Rubenstein, J. L. R. and Yang, Z. (2012). A subpopulation of dorsal lateral/caudal ganglionic eminence-derived neocortical interneurons expresses the transcription factor Sp8. *Cereb. Cortex* **22**, 2120-2130.
Magnusson, J. P., Göritz, C., Tatarishvili, J., Dias D. O., Smith E. M. K., Lindvall, O., Kokaia, Z. and Frisén J. (2014). A latent neurogenic program in astrocytes regulated by Notch signaling in the mouse. *Science* **346**, 237-241.
Merkle, F. T., Mirzadeh, Z. and Alvarez-Buylla, A. (2007). Mosaic organization of neural stem cells in the adult brain. *Science* **317**, 381-384.
Merkle, F. T., Fuentealba, L. C., Sanders, T. A., Magno, L., Kessaris, N. and Alvarez-Buylla, A. (2014). Adult neural stem cells in distinct microdomains generate previously unknown interneuron types. *Nat. Neurosci.* **17**, 207-214.
Mori, T., Tanaka, K., Buffo, A., Wurst, W., Kühn, R. and Götz, M. (2006). Inducible gene deletion in astroglia and radial glia–a valuable tool for functional and lineage analysis. *Glia* **54**, 21-34.
Ninkovic, J. and Götz, M. (2013). Fate specification in the adult brain–lessons for eliciting neurogenesis from glial cells. *Bioessays* **35**, 242-252.
Niu, W., Zang, T., Zou, Y., Fang, S., Smith, D. K., Bachoo, R. and Zhang, C.-L. (2013). In vivo reprogramming of astrocytes to neuroblasts in the adult brain. *Nat. Cell Biol.* **15**, 1164-1175.
Peitz, M., Pfannkuche, K., Rajewsky, K. and Edenhofer, F. (2002). Ability of the hydrophobic FGF and basic TAT peptides to promote cellular uptake of recombinant Cre recombinase: a tool for efficient genetic engineering of mammalian genomes. *Proc. Natl. Acad. Sci. USA* **99**, 4489-4494.
Peng, H., Bria, A., Zhou, Z., Iannello, G. and Long, F. (2014). Extensible visualization and analysis for multidimensional images using Vaa3D. *Nat. Protoc.* **9**, 193-208.
Ohira, K., Furuta, T., Hioki, H., Nakamura, K. C., Kuramoto, E., Tanaka, Y., Funatsu, N., Shimizu, K., Oishi, T., Hayashi, M. et al. (2010). Ischemia-induced neurogenesis of neocortical layer 1 progenitor cells. *Nat. Neurosci.* **13**, 173-179.
Parras, C. M., Galli, R., Britz, O., Soares, S., Galichet, C., Battiste, J., Johnson, J. E., Nakafuku, M., Vescovi, A. and Guillemot, F. (2004). Mash1 specifies neurons and oligodendrocytes in the postnatal brain. *EMBO J.* **23**, 4495-4505.
Pastrana, E., Cheng, L.-C. and Doetsch, F. (2009). Simultaneous prospective purification of adult subventricular zone neural stem cells and their progeny. *Proc. Natl. Acad. Sci. USA* **106**, 6387-6392.
Platel, J.-C., Gordon, V., Heintz, T. and Bordey, A. (2009). GFAP-GFP neural progenitors are antigenically homogeneous and anchored in their enclosed mosaic niche. *Glia* **57**, 66-78.
Preibisch, S., Saalfeld, S. and Tomancak, P. (2009). Globally optimal stitching of tiled 3D microscopic image acquisitions. *Bioinformatics* **25,** 1463-1465.
Shihabuddin, L. S., Horner, P. J., Ray, J. and Gage, F. H. (2000). Adult spinal cord stem cells generate neurons after transplantation in the adult dentate gyrus. *J. Neurosci.* **20**, 8727-8735.
Sirko, S., Behrendt, G., Johansson, P. A., Tripathi, P., Costa, M. R., Bek, S., Heinrich, C., Tiedt, S., Colak, D., Dichgans, M. et al. (2013). Reactive glia in the injured brain acquire stem cell properties in response to sonic hedgehog glia. *Cell Stem Cell* **12**, 426-439.
Srinivas, S., Watanabe, T., Lin, C.-S., William, C. M., Tanabe, Y., Jessell, T. M. and Costantini, F. (2001). Cre reporter strains produced by targeted insertion of EYFP and ECFP into the ROSA26 locus. *BMC Dev. Biol.* **1**, 4.
Waclaw, R. R., Allen, Z. J., Bell, S. M., Erdélyi, F., Szabó, G., Potter, S. S. and Campbell, K. (2006). The zinc finger transcription factor Sp8 regulates the generation and diversity of olfactory bulb interneurons. *Neuron* **49**, 503-516.
Wearne, S. L., Rodriguez, A., Ehlenberger, D. B., Rocher, A. B., Henderson, S. C. and Hof, P. R. (2005). New Techniques for imaging, digitization and analysis of three-dimensional neural morphology on multiple scales. *Neuroscience* **136**, 661-680.
Zhu, X., Hill, R. A., Dietrich, D., Komitova, M., Suzuki, R. and Nishiyama, A. (2011). Age-dependent fate and lineage restriction of single NG2 cells. *Development* **138**, 745-753.
Zhuo, L., Sun, B., Zhang, C. L., Fine, A., Chiu, S. Y. and Messing, A. (1997). Live astrocytes visualized by green fluorescent protein in transgenic mice. *Dev. Biol.* **187**, 36-42.

Supplementary Figures

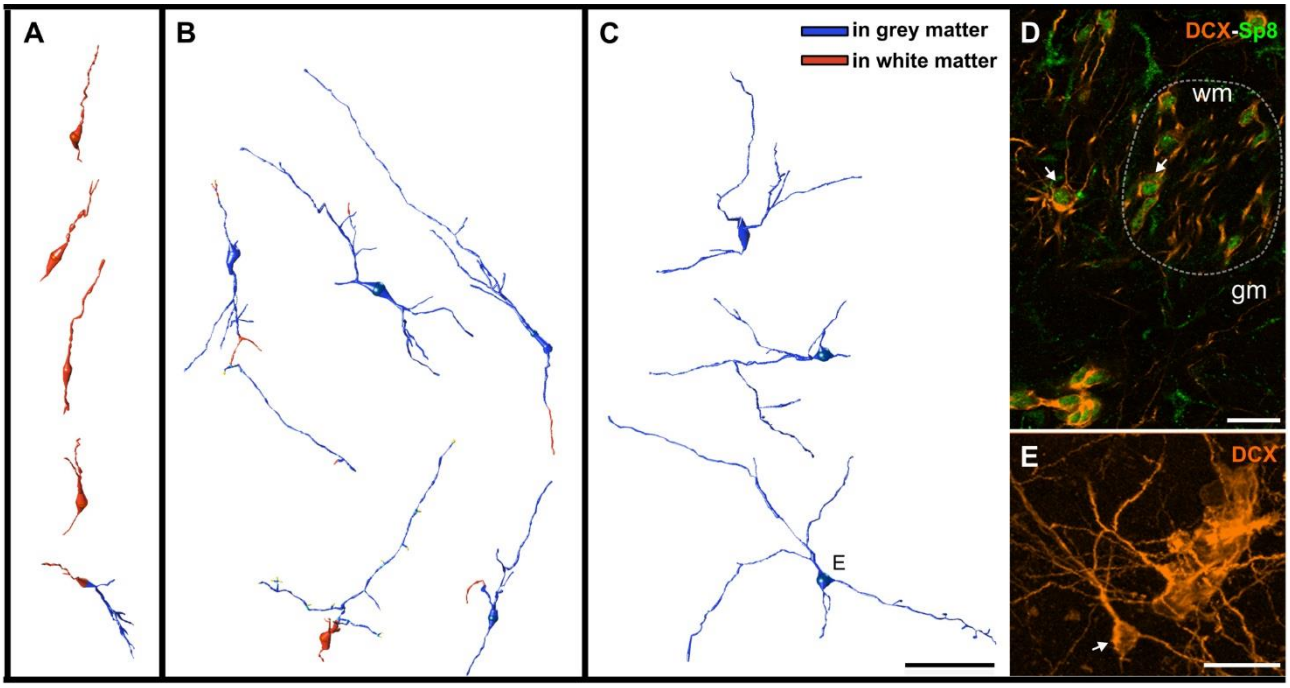

Supplementary Fig.1) Phenotypic analysis of DCX$^+$ cells in the 5w.p.l striatum. **a-c)** Threedimensional reconstructions of DCX$^+$ neuroblasts. According with their complexity and with the presence of processes in the grey (blue) and white (red) matter we divided these cells in three categories. **a)** Cells with short unbranched processes: most such cells were associated with the white matter and showed the characteristic bipolar morphology of migrating neuroblasts. **b)** Cells with long and branched processes running in both white and grey matter. **c)** Cells with long and branched processes running exclusively in the grey matter. It is to note that although most cells associated mainly with the white matter were bipolar, some showed a more elaborated morphology. However, these few cells were surrounded by a high density of cells and processes that hampered the complete reconstruction of their morphology. **d**) Single confocal slice showing the expression of SP8 (green) in DCX$^+$ cells (orange). Note that this transcription factors is expressed in both cD (arrowhead) and iD (arrows) cells in both grey and white matter (dotted line). **e**) Z projection of part of the stack containing one of the reconstructed cells (arrow) shown in **d**. Scale Bars: 40µm in **a-c**, 20 µm in **d,e**.

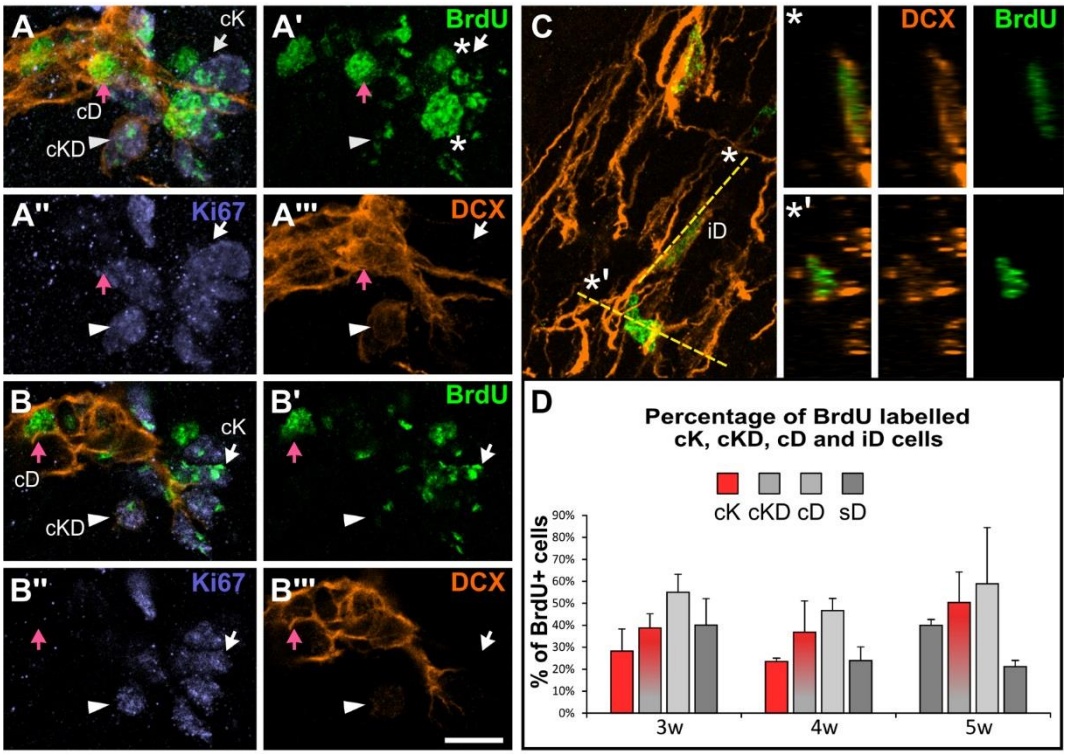

Supplementary Fig.2) *BrdU labelling among induced striatal Ki67$^+$ clusters and DCX$^+$ neuroblasts.* **a-b**) Zprojection (**b-b'''**) and single confocal plane (**c-c'''**) of a Ki67$^+$ (violet) cluster partially overlapped with a DCX$^+$ (orange) cluster showing examples of cK (white arrow), cKD (white arrowhead) and cD (pink arrow) cells labelled by BrdU, four days after administration (green). The fragmented BrdU staining in the Ki67$^+$ cells suggests that these cells are actively dividing. **c**) Some individual DCX$^+$ cells (iD) are also labelled for BrdU (pink arrowhead). For two such cells a reslice along the plane indicated by a dotted line is indicated (***, *'**). **d**) Percentages ±S.D. of BrdU$^+$ cells among cK, cKD, cD and iD cells cells at 3, 4, 5w.p.l., n=4. Error bars indicate standard deviation. Scale bars: 10µm.

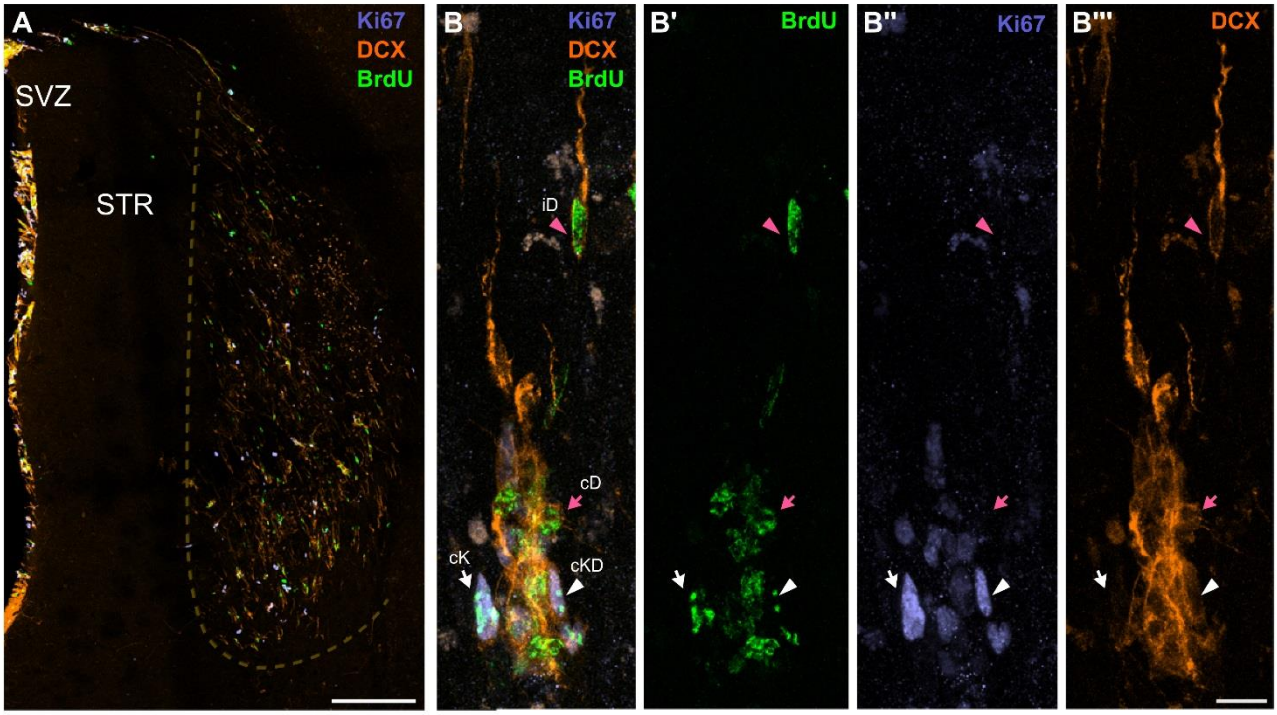

Supplementary Fig.3) The QA lesion induces a long lasting neurogenic response. **a**) Coronal section of an animal sacrificed *6 month after QA lesion* showing striatal Ki67$^+$ *(violet)* and DCX$^+$ *(orange)* cells in the striatum, mostly located within the lesioned area (yellow dotted line). Several Ki67$^+$ and DCX$^+$ cells incorporated the BrdU (green) injected four days before the sacrifice. **b-b''**) Confocal stack showing an higher magnification of Ki67 and DCX$^+$ cells in the lesioned striatum. These cells include a cluster of cK (white arrow), cKD (white arrowhead) and cD (pink arrow) cells as well as iD (pink arrowhead) cells. Note that all cell types are partly labelled for BrdU. Scale bars: 200µm in **a**; 10µm in **b-b'.**

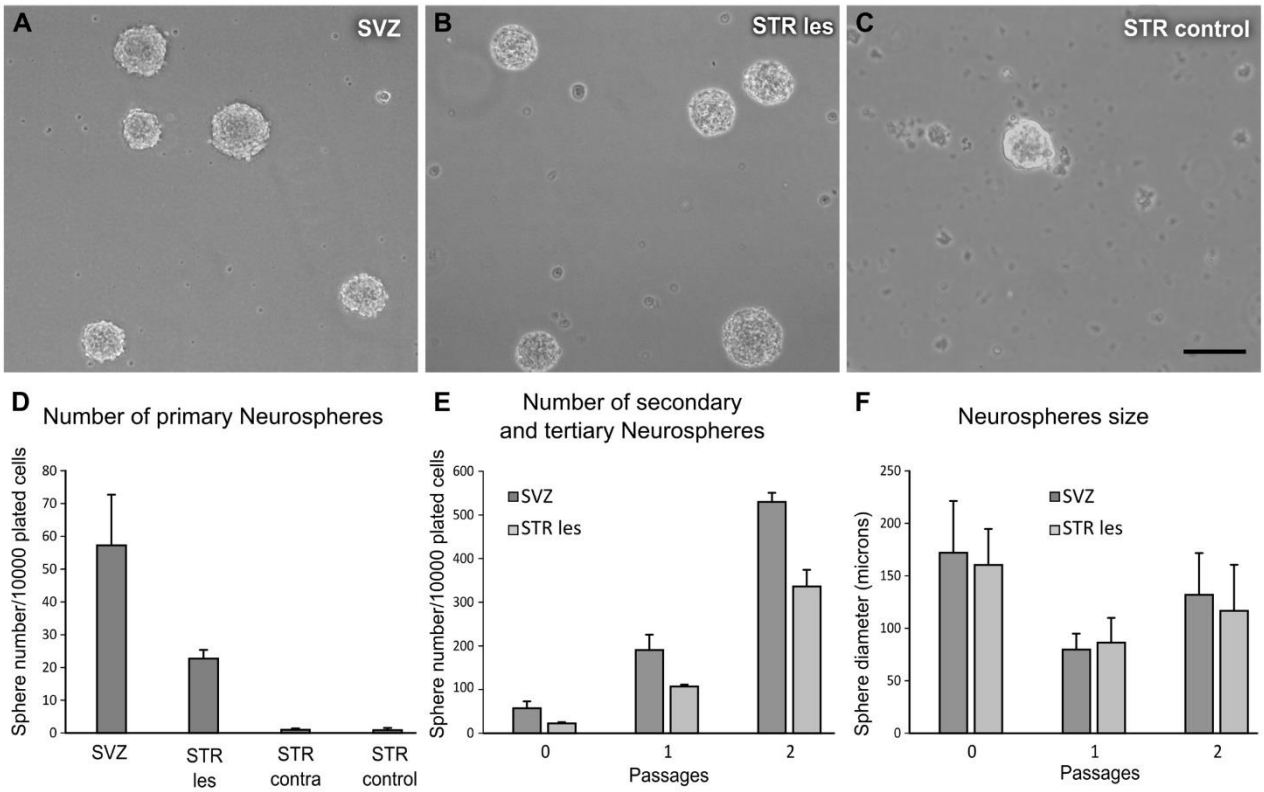

Supplementary Fig.4) *Neurosphere assay*. **a-c**) Representative images of primary neurospheres isolated from intact SVZ (**a**), lesioned striatum (STR les; **b**), and intact striatum (STR control; **c**). **d**) Number of primary neurospheres isolated from SVZ, lesioned striatum, striatum contralateral to the QA injection (STR contra) and intact striatum from non lesioned animals of a representative experiment. Bars indicate the mean values ±S.E.M. of the number of neurospheres for 10000 plated cells; n=4 dishes for each case). **e**) The number of SVZ and STR les derived neurospheres steeply increase during the first two *in vitro* passages while the neurospheres diameter remain constant (**f**). Scale bar: 150µm.

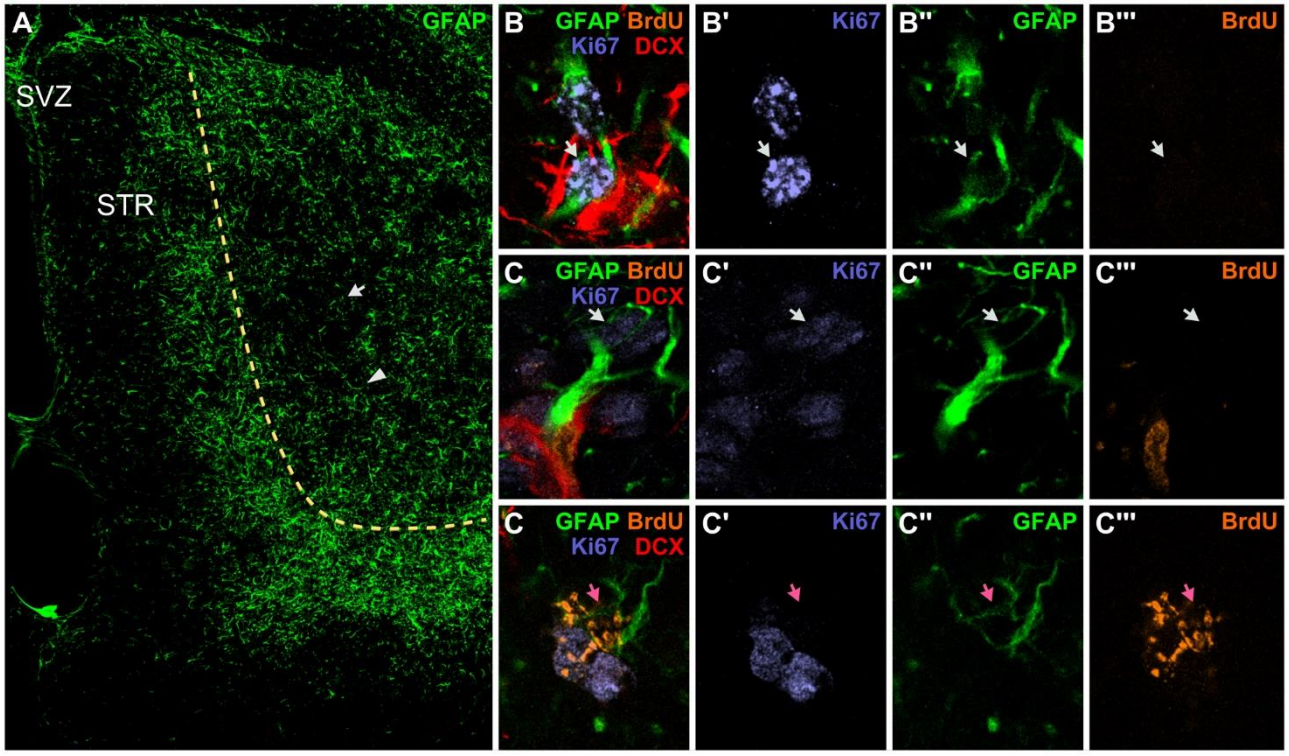

Supplementary Fig.5) Proliferation of striatal GFAP$^+$ astrocytes. a) Coronal section of a 5w.p.l. striatum showing the staining of GFAP (green). In contrast to control animals, GFAP is strongly expressed by striatal astrocytes after lesion, particularly at the lesion border (dotted line). b) Single confocal plane showing a GFAP$^+$ (green) cell labelled by Ki67$^+$ (violet) but not DCX (red) nor BrdU (orange; white arrow). Note that this cell is close to a second Ki67$^+$ cells in which the positivity for GFAP cannot be clearly established. *c)* Single confocal plane showing a GFAP$^+$ cell labelled by Ki67$^+$ in a cluster comprising cK (white arrow), cKD and cD cells. d) Single confocal plane showing a GFAP$^+$ cell labelled by BrdU (pink arrow). This cell was closely associated to a cluster of cK cells (two of which are visible in this focal plane) that were also mostly labelled for BrdU. Scale Bars: 200 μm in a, 10μm in b-d.

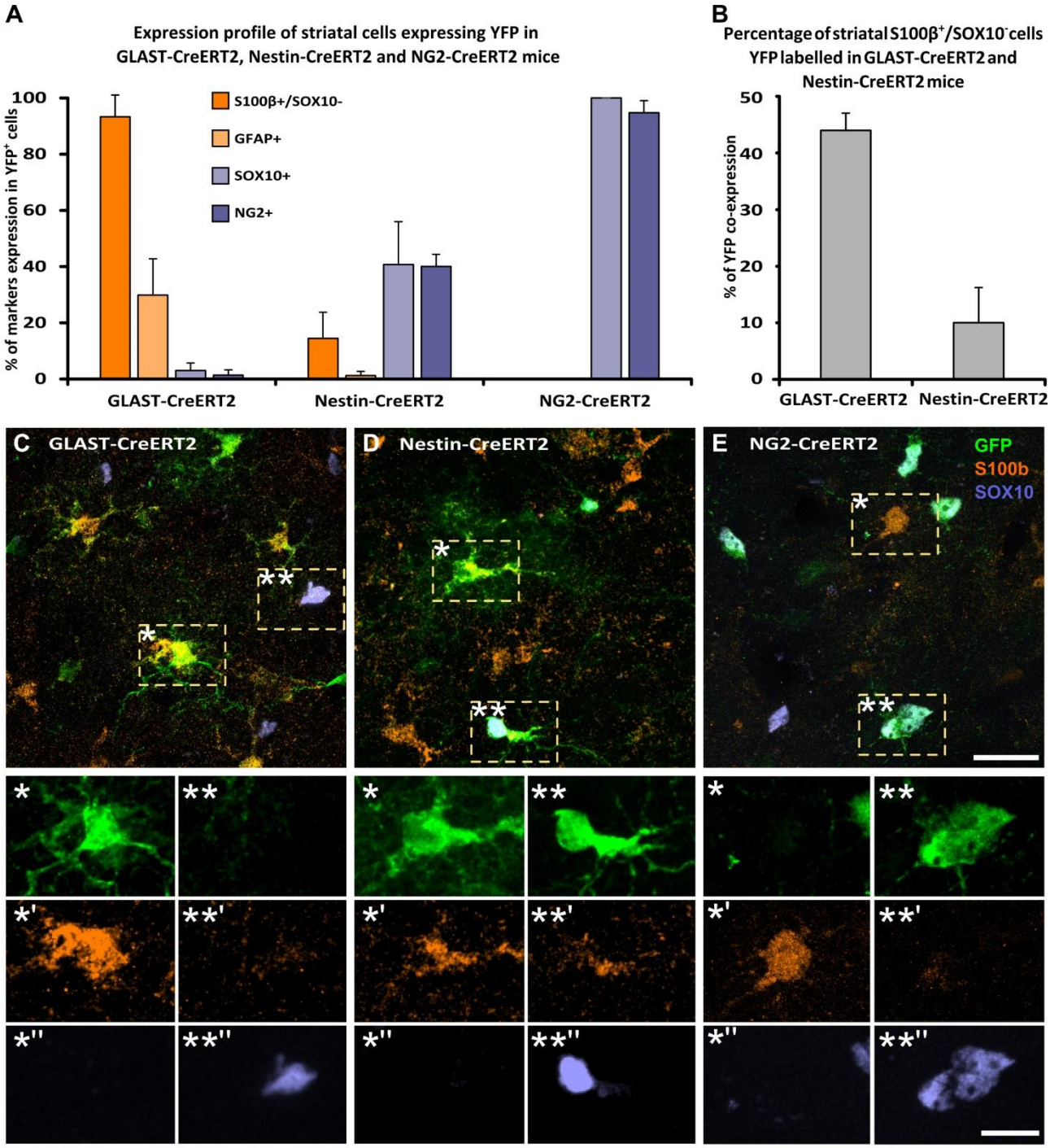

Supplementary Figure 6) Phenotypic analysis of recombined cells in the intact striatum of GLAST, Nestin and NG2-CreER^{T2} animals. **a**) Percentage of YFP$^+$ cells expressing markers of the astroglial (S100β, GFAP) or oligodendroglial (NG2, SOX10) lineages in the intact striatum of GLAST, Nestin and NG2-CreER^{T2} animals either one week (for GLAST-CreER^{T2} and Nestin-CreER^{T2}) or two weeks (for NG2) after tamoxifen administration. Since part of the S100β cells co-expressed SOX10, only the S100β$^+$/SOX10$^-$ cells were considered as astroglia. As expected, YFP$^+$ cells were almost exclusively represented by astrocytes in GLASTCreER^{T2} animals, by a mixture of astroglial and oligodendroglial cells in Nestin-CreER^{T2} animals and exclusively by oligodendroglial cells in NG2-CreER^{T2} animals. It is to note that only a small percentage of YFP$^+$ cells co-express GFAP, and this is consistent with the low expression of this protein in the intact parenchyma. **b)** Fraction of recombined S100β$^+$/SOX10$^-$ astrocytes in GLAST-CreER^{T2} and Nestin-CreER^{T2} animals. **c-d**)

Confocal stacks of the intact striatum of GLAST-CreER^{T2} (c), NestinCreER^{T2} (d) and NG2-CreER^{T2} mice (e) showing the expression YFP (green) in S100β^{+} (orange, *) or SOX10^{+} (violet, **) cells. Note that the expression of SOX10 or S100β in YFP^{+} cells closely correlate with the occurrence of morphological features characteristic of the oligodendroglial or astroglial lineages, respectively. Error bars indicate standard deviation. Scale bars: 20μm in **b, c, d**; 10μm in higher magnifications

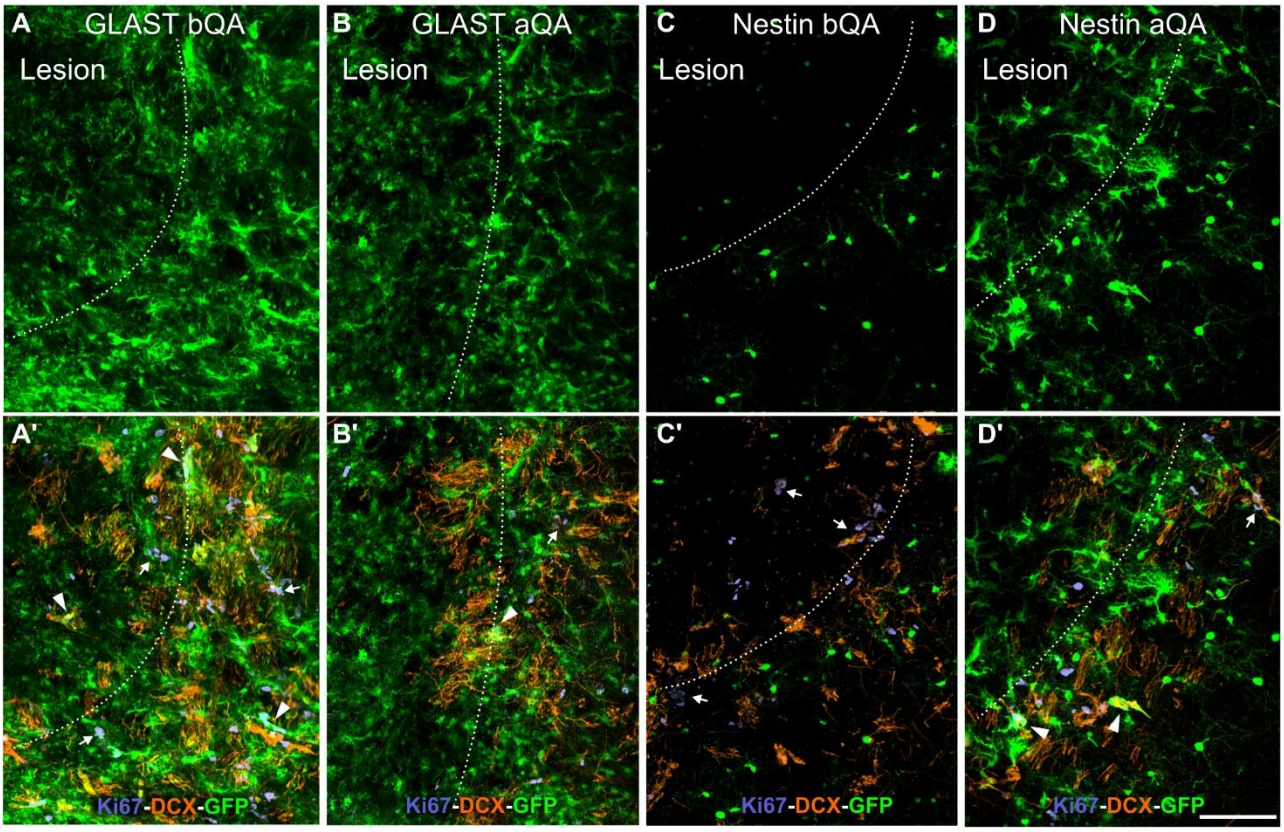

Supplementary Fig.7) *Distribution of YFP$^+$ cells in the striatum of fate mapped animals*. **ad**) YFP (green) Ki67 (violet) and DCX (orange) staining in representative 50µm coronal sections of 5w.p.l. striatum at the level of the lesion border (dotted line) of GLAST-CreER^{T2} bQA (**a,a'**), GLAST-CreER^{T2} aQA (**b,b'**), Nestin-CreER^{T2} bQA (**c,c'**) and Nestin-CreER^{T2} aQA animals. Note that numerous GFP$^+$ cells can be observed at the lesion border of both GLAST-CreER^{T2} bQA and aQA animals. By contrast, in Nestin-CreER^{T2} bQA animals only few YFP$^+$ cells can be observed, and according to their characteristic morphology these elements represent mostly oligodendrocytes and to a lesser extent neurons. Similar cells can be observed also in Nestin-CreER^{T2} aQA animals together with numerous cells with astrocytic morphology mostly distributed at the lesion border, where most Ki67$^+$ and DCX$^+$ clusters were located. In **a'-d'** also note that only a fraction of Ki67$^+$ clusters contains GFP$^+$ cells (arrowhead and arrow indicate respectively recombined and non recombined Ki67$^+$ clusters). Scale bar: 100µm.

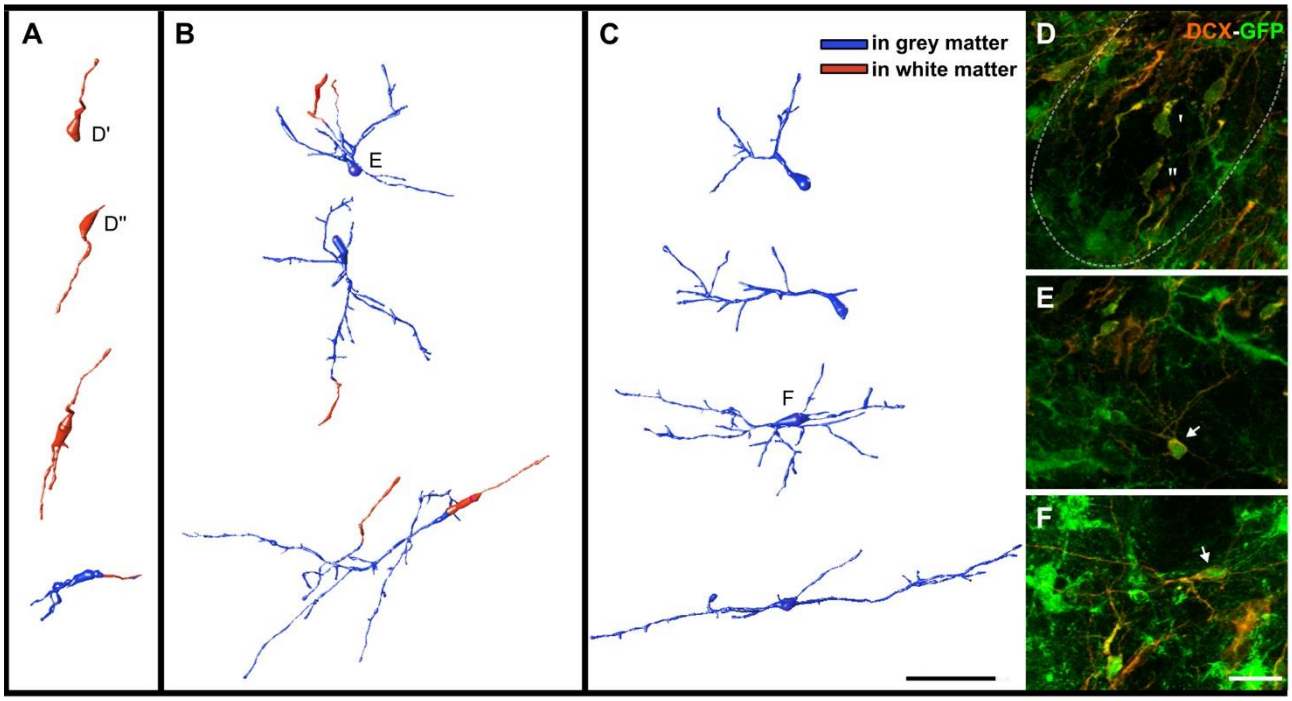

Supplementary Figure 8) Three dimensional reconstruction of DCX$^+$/YFP$^+$ cells in the 5w.p.l striatum of GLAST-CreER^{T2} bQA animals **a-c)** Three-dimensional reconstructions of DCX$^+$ neuroblasts that expressed YFP in the 5w.p.l striatum of GLAST-CreER^{T2} animals treated with tamoxifen one week before QA lesion. The morphology of these cells were consistent with the categories of DCX$^+$ neuroblasts previously described in supplementary Fig.1 **d-f**) Z projection of part of the stack containing some of the reconstructed cells shown in **a-c**. Scale Bars: 40µm in **a-c**, 20 µm in **d, e.**

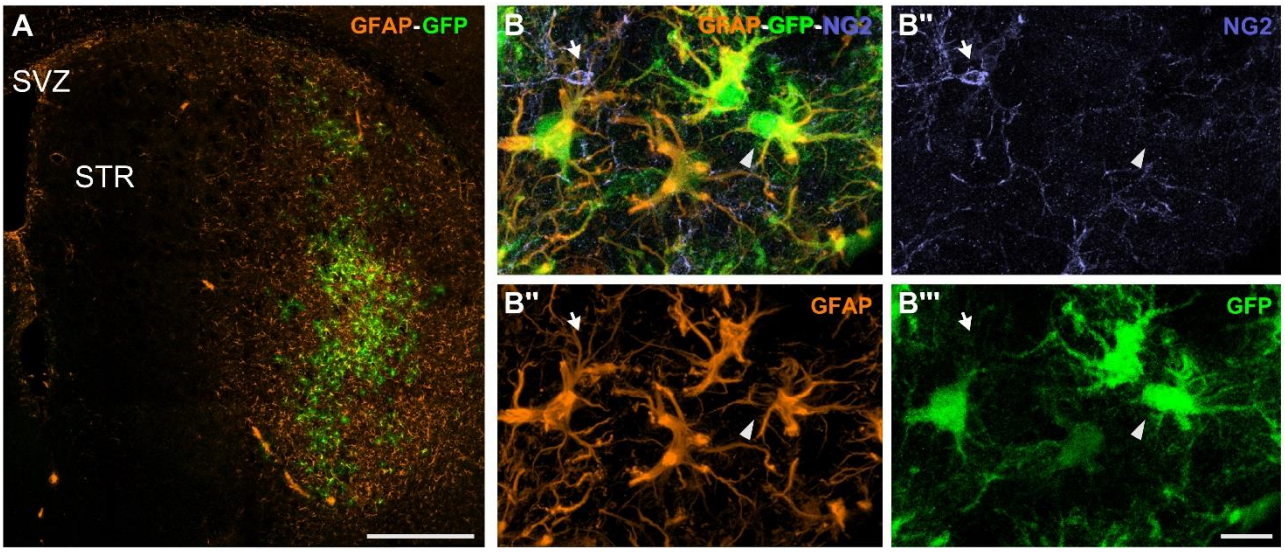

Supplementary Fig.9) Phenotypic analysis of recombined cells in the intact striatum of R26R animals receiving Ad:GFAP-Cre injections. **a)** Coronal section at the level of the striatum labelled for GFAP (orange) and GFP (green). Note that the GFP^+ cells are restricted to the ventro-lateral striatum and that the injection of the viral vector consistently induced the expression of GFAP at the level of the injection site and surrounding area of the striatum. The reactivity of astrocytes is consistent with previous work showing that intracerebral injections of adenoviral vectors induce an inflammatory response (Lowenstein and Castro, 2003). **b)** Z-Projection of a confocal stack at the level of the injection site showing that recombined cells expressing YFP (green) co-express GFAP (orange, arrowhead) but not NG2 (violet, arrow). Quantitative analyses indicated that no YFP^+ cells in the striatum of these animals expressed NG2 and the 93±5% (n=3) expressed GFAP. Scale Bars: 200 μm in **a**, 20 μm in **b**.

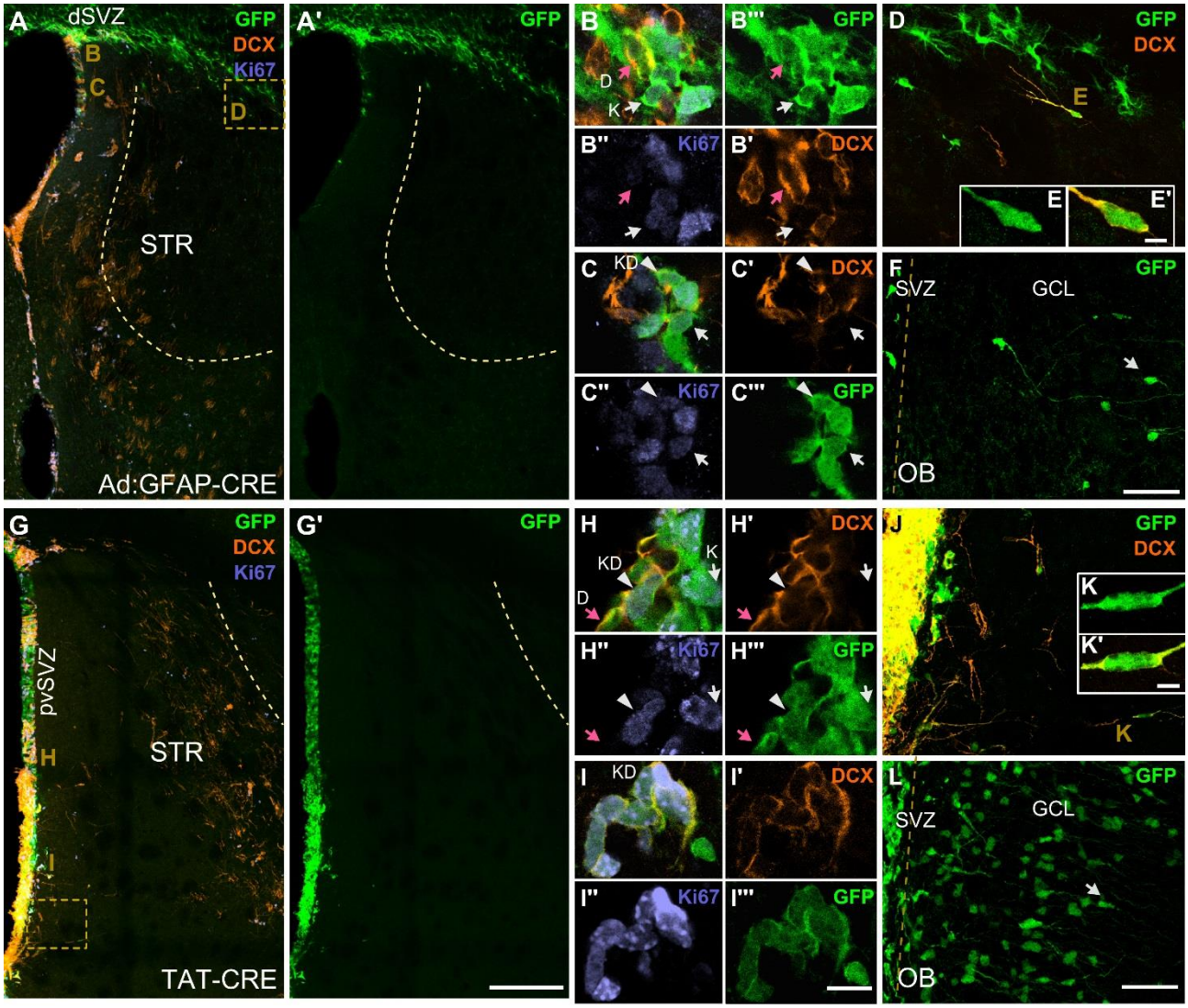

Supplementary Fig.10) SVZ contribution to QA lesion induced neurogenesis. **a-f)** Coronal sections at the level of the central striatum (a, and higher magnifications in b-d) and olfactory bulb (f) of a 5w.p.l R26R reporter mice injected with Ad:GFAP-Cre one week before QA. **g-l)** coronal sections at the level of the anterior striatum (g, and higher magnifications in h-j) and olfactory bulb (l) of a 5w.p.l R26R reporter mice injected with TAT-Cre one week before QA. The injection of the Ad:GFAP-Cre and TAT-Cre induced widespread expression of YFP (green) respectively in in the dorso-lateral parts of the SVZ (dSVZ, a) and its peri-ventricular regions (pvSVZ, g). As shown by higher magnification of single confocal planes, YFP^+ cells in both the dSVZ (b) and pvSVZ (c,h) include putative TAPs expressing Ki67 (violet) but not DCX (orange, white arrow), as well as proliferating (white arrowhead) and post-mitotic (pink arrow) DCX^+ neuroblasts. In addition for both injection protocols many YFP^+ cells could be observed in the OB (white arrows) f,l). Collectively these observations indicate that our approach consistently labelled longlasting primary neuronal progenitors of all SVZ sub-regions. Nonetheless in the striatum of these animals we could identify only few YFP^+ iD cells (d, e and j, k) and these cells were generally located within 200µm from the SVZ. It is to note that a few clusters of $Ki67^+$ and YFP^+ cells were occasionally observed in TAT-Cre injected animals (i), particularily at anterior levels of the striatum. However these clusters were mostly made by cKD cells and were always located at less than 50µm from the SVZ. Scale Bars 200µm in a-g, 50 µm in
d, f, j, l, 10 µm in b, c, ,h, l, 5 µm in e-k.

Supplementary Table 1) Analysis of *YFP expression in Ki67$^+$ and DCX$^+$ cells in the SVZ and striatum of GLAST and Nestin-CreER^{T2} animals, in bQa and aQA condition.*

In the table are reported the values of statistical tests performed on the percentage of YFP$^+$ cells among different striatal (STR) and SVZ cell types shown in Fig.2**a**. For ANOVA analyses that returned statistically significant values, tukey post-hoc tests are also shown. **a)** *Within region comparisons*. Percentage of YFP$^+$ cells among distinct cell types is compared within the SVZ and STR. Note that in both GLAST-CreER^{T2} bQA and Nestin-CreER^{T2} bQA animals the fraction of YFP$^+$ elements among the considered cell types in each region is not statistically different. By contrast, in GLAST-CreER^{T2} aQA animals, in both SVZ and STR, the proliferating cells (SVZ: Ksvz, KDsvz; STR: cK, cKD) show a higher value of YFP coexpression in respect to postmitotic elements (SVZ: Dsvz; STR: cD, iD; see Fig.2A). Nestin-CreER^{T2} aQA animals show a similar trend, although in both SVZ and STR only the Ki67$^+$/DCX cells (SVZ: Ksvz; STR: cK) contain a significantly higher fraction of YFP$^+$ cells. **b)** *Between regions comparisons*. The different cell types are compared between SVZ and STR. Note that in GLAST-CreER^{T2} bQA animals cK, cKD and cD cells show lower percentage of recombination in respect to the corresponding cell types in the SVZ (Ksvz, KDsvz and Dsvz). possibly due to different efficiency of GLAST-driven recombination among SVZ and striatal astrocytes. **c)** *Between groups comparisons*. The fraction of YFP$^+$ cells for all considered cell types is compared before and after tamoxifen among different strains (GLAST-CreER^{T2} bQA vs Nestin-CreER^{T2} bQA; GLAST-CreER^{T2} aQA vs Nestin-CreER^{T2} aQA), or in the same strain (Nestin-CreER^{T2} bQA vs Nestin-CreER^{T2}aQA; GLAST-CreER^{T2} bQA vs GLAST-CreER^{T2} aQA). Note that in the SVZ the percentage of YFP$^+$ cells does not differ between strains, indicating similar efficiency of Nestin- or GLAST-driven recombination in primary progenitors. By contrast, in the striatum all cell types show higher level of recombination in GLAST-CreER^{T2} bQA than in Nestin-CreER^{T2} bQA animals. This difference is lost in the aQA condition, accordingly to the significant increase of cK and cKD cells in Nestin-CreER^{T2} aQA, in respect to Nestin-CreER^{T2} bQA animals.

a) Within Regions Comparisons

	Compared Cell types	STATISTICAL TEST	GLAST-bQA	Nestin-bQA	GLAST-aQA	Nestin-aQA
SVZ	K_{SVZ} vs KD_{SVZ} vs D_{SVZ}	One way ANOVA	$F_{(2,6)}$=0,342 p=0,723	$F_{(2,9)}$=1,432 p=0,288	$F_{(2,6)}$=21,734 p=0,002	$F_{(3,12)}$=5,597 p=0,012
	K_{SVZ} vs KD_{SVZ}	Tukey post hoc	-	-	p=0,051	p=0,024
	K_{SVZ} vs D_{SVZ}	Tukey post hoc			p=0,001	p=0,026
	KD_{SVZ} vs D_{SVZ}	Tukey post hoc			p=0,028	p=0,998
STR	cK vs cKD vs cD vs iD	One way ANOVA	$F_{(3,8)}$=2,032 p=0,188	$F_{(3,12)}$=2,713 p=0,092	$F_{(3,8)}$=9,802 p=0,005	$F_{(3,12)}$=5,597 p=0,012
	cK vs cKD	Tukey post hoc	-	-	p=1,000	p=0,076
	cK vs cD	Tukey post hoc			p=0,027	p=0,020
	cK vs iD	Tukey post hoc			p=0,016	p=0,036
	cKD vs cD	Tukey post hoc			p=0,027	p=0,670
	cKD vs iD	Tukey post hoc			p=0,016	p=0,849
	cD vs iD	Tukey post hoc			p=0,979	p=0,990

b) Between Regions Comparisons

	Compared Cell types	STATISTICAL TEST	GLAST-bQA	Nestin-bQA	GLAST-aQA	Nestin-aQA
STR vs SVZ	K_{SVZ} vs cK_{SVZ}	T-Test	p=0,038	p<0,001	p=0,020	p=0,372
	KD_{SVZ} vs cKD	T-Test	p=0,016	p=0,001	p=0,380	p=1,000
	D_{SVZ} vs cD vs iD	One way ANOVA	$F_{(2,6)}$=10,599 p=0,011	$F_{(2,9)}$=35,737 p<0,001	$F_{(2,6)}$=3,198 p=0,113	$F_{(2,6)}$=1,960 p=0,221
	D_{SVZ} vs cD	Tukey post hoc	p=0,009	p<0,001	-	-
	D_{SVZ} vs iD	Tukey post hoc	p=0,189	p<0,001		
	cD vs iD	Tukey post hoc	p=0,092	p=0,409		

c) Between Groups Comparisons

	Compared Cell types	STATISTICAL TEST	GLAST-bQA vs Nestin-bQA	GLAST-aQA vs Nestin-aQA	GLAST-bQA vs GLAST-aQA	Nestin-bQA vs Nestin-aQA
SVZ	K_{SVZ}	T-Test	p=0,110	p=0,142	p=0,019	p=0,030
	KD_{SVZ}	T-Test	p=0,068	p=0,049	p=0,004	p<0,001
	D_{SVZ}	T-Test	p=0,899	p=0,577	p<0,001	p<0,001
STR	ck	T-Test	p=0,002	p=0,477	p=0,060	p=0,015
	cKD	T-Test	p=0,049	p=0,153	p=0,241	p=0,030
	cD	T-Test	p=0,010	p=0,838	p=0,017	p=0,605
	iD	T-Test	p=0,015	p=0,069	p=0,011	p=0,298

Table S2. Antibodies

ANTIGEN NAME	HOST	DILUTION	SOURCE	STOCK NUMBER
Primary antisera				
ASCL-1	Mouse	1:500	BD Pharmingen	556604
BrdU	Rat	1:3000	AbD Serotec	OBT0030CX
DCX	Goat	1:1500	Santa Cruz Biotechnology	Sc-8066
GFAP	Rabbit	1:2000	Dako	Z 0334
GFP	Chicken	1:1000	Aveslab	GFP-1020
Ki67	Rabbit	1:1000	Novocastra	NCL-Ki67p
Ki67	Mouse	1:500	BD Pharmingen	550609
NeuN	Mouse	1:1000	Chemicon	MAB377
NG2	Rabbit	1:500	Chemicon	AB5320
O4	Mouse	1:200	Millipore	MAB345
S100β	Rabbit	1:10000	Swant	37A
SOX-10	Goat	1:1000	Santa Cruz Biotechnology	Sc-17342
SOX-9	Rabbit	1:1000	Millipore	AB5535
Sp8	Rabbit	1:10000	Millipore	AB15260
Tuj1	Mouse	1:1500	Sigma	T8660
Secondary antisera				
Cy3 Anti-Rb	Donkey	1:800	Jackson ImmunoResearch	711-165-152
Cy3 Anti-Ms	Donkey	1:800	Jackson ImmunoResearch	715-165-151
Cy3 Anti-Gt	Donkey	1:800	Jackson ImmunoResearch	705-165-147
Cy3 Anti-Rt	Donkey	1:800	Jackson ImmunoResearch	712-165-153
AlexaFluor488 Anti-Rb	Donkey	1:400	Jackson ImmunoResearch	711-545-152
AlexaFluor488 Anti-Ms	Donkey	1:400	Jackson ImmunoResearch	715-545-151
AlexaFluor488 Anti-Gt	Donkey	1:400	Jackson ImmunoResearch	705-545-147
AlexaFluor488 Anti-Rt	Donkey	1:400	Jackson ImmunoResearch	712-545-153
AlexaFluor488 Anti-Ck	Donkey	1:400	Jackson ImmunoResearch	703-545-155
AlexaFluor647 Anti-Rb	Donkey	1:600	Jackson ImmunoResearch	711-605-152
AlexaFluor647 Anti-Ms	Donkey	1:600	Jackson ImmunoResearch	715-605-151
AlexaFluor647 Anti-Gt	Donkey	1:600	Jackson ImmunoResearch	705-605-147
AlexaFluor647 Anti-Rt	Donkey	1:600	Jackson ImmunoResearch	712-605-153
Biotynilated Anti-Rat	Rabbit	1:150	Vector Laboratories	BA-4001
AMCA-avidinD		1:100	Vector Laboratories	A-2008

Supplementary materials and methods

Transgenic Mouse lines

Experiments were performed on 8-12 weeks animals of the following mouse lines: C57BL/6 mice (Harlan laboratories), GLAST-CreER^{T2} (Mori et al., 2006), Nestin-CreER^{T2} (Corsini et al., 2009), NG2-CreER^{T2} (B6.Cg-Tg/Cspg4-Cre/Esr1*/BAkik/J; Jackson Labs; Zhu et al., 2011), R26R-YFP (Srinivas et al., 2001) and hGFAP-GFP (Zhuo et al., 1997); FVB/N-TgGFAPGFP14Mes/J; Jackson Labs) animals . Nestin-CreER^{T2}, GLAST-CreER^{T2} and NG2-CreER^{T2}) were crossed to R26R-YFP mice to produce: Nestin-CreER^{T2}/R26R-YFP and NG2-CreER^{T2}/R26R-YFP mice hemizygous for both genes and GLAST-CreER^{T2}/R26R-YFP mice heterozygous for GLAST-CreER^{T2} and homozygous for R26R:YFP.

Neurosphere assay

Lesioned striatum, healty striatum and subventricular zone (SVZ; n=4 per experiment) were dissected, dissociated and cultured (10000 cells/mL) in a standard neurosphere assay (Pastrana et al., 2009). For each group the rate of neurosphere generation was determined as the number of primary neurospheres by the number of viable seeded cells. Self-renewal of SVZ and STR-les was determined as the number of neurospheres/number of viable seeded cells derived from spheres of the previous passage. The number of neurospheres was determined after 7 days of culture. Diameters of living neurospheres were measured using ImageJ software. Three replicates were performed. For assessment of differentiation, neurospheres were plated onto polyD-lysine coated coverslip coated in differentiation medium. Plated cells were processed 7 days later using immunocytochemistry: we used anti-GFAP, anti-βIIItubulin and anti-O4 to determine astroglial, neuronal and oligodendroglial differentiation, respectively

Quantifications and statistical analyses

All countings were performed in ImageJ on sections acquired at the confocal microscope (voxel size: 0.35µm x 0.35µm x 1.50µm).

Stereological evaluation of the number, organization and BrdU labelling of DCX$^+$ and Ki67$^+$ cells. This analysis was performed in the six central focal planes of two non-consecutive 50µm thick slices. The DCX$^+$ and Ki67$^+$ clusters were defined as

groups of at least four cells with closely contacting cell bodies and expressing the same marker. For double-labelled cells, clustering has been evaluated separately for each marker.

Expression of ASCL1 (n=2), SOX9 (n=2) and GFAP-GFP (n=3) in striatal cK, cKD, cD, iD cells was evaluated in 3-4 slices. The number of counted cell per animal ranged from 55 to 100 cells for cK, 182 to 206 for cKD. For iD and cD 100 cells per animal were counted.

Genetic fate-mapping analysis of SVZ and striatal cells: Analyses were performed in Nestin-CreER^{T2} (Nestin-CreER^{T2} bQA n=4, Nestin-CreER^{T2} aQA n=5) and GLAST-CreER^{T2} animals (GLAST-CreER^{T2} bQA n=3, GLAST-CreER^{T2} aQA n=3). In the SVZ, the percentage of recombined Ki67^{+}/DCX^{-} (K_{SVZ}), Ki67^{+}/DCX^{+} (KD_{SVZ}), and Ki67^{+}/DCX^{+} (D_{SVZ}) were counted at the level of the rostral migratory stream (RMS) in hemispheres ipsilateral to the lesion. Counted cells ranged from 64 to 165 for K_{SVZ} cells; from 54 to 144 for KD_{SVZ} cells and from 332 to 888 for D_{SVZ} cells). In the striatum, fractions of GFP^{+} cK, cKD, and iD cells were counted over the entire thickness of 2-4 sections while cD cells were counted in two non-consecutive focal planes. Counted cells ranged from 77 to 473 for cK cells, from 85 to 474 for cKD cells, from 82 to 192 for cD cells and from 460 to 1160 for iD cells.

Cell composition of reporter^{+} Ki67^{+} clusters in fate-mapped animals. This analysis was performed on randomly selected Ki67^{+} clusters that contained at least a single reporter^{+} cell. Selected clusters were entirely reconstructed from subsequent sections and the number of reporter^{+} and reporter^{-} cells were counted. The number of Ki67^{+} clusters that were composed by 100% reporter^{+} cells over the total number of analyzed clusters were as follows: GLAST-CreER^{T2} bQA, 35/39; GLAST-CreER^{T2} aQA 21/24 Nestin-CreER^{T2} bQA 8/8, Nestin-CreER^{T2} aQA 20/31; VSVG-GFP 17/18; Ad:GFAP-Cre 11/12.

Statistical analyses were performed in SPSS 19. Anova analyses that returned significant F values were followed by Tukey's post hoc tests.

References

Corsini, N. S., Sancho-Martinez, I., Laudenklos, S., Glagow, D., Kumar, S., Letellier, E., Koch, P., Teodorczyk, M., Kleber, S., Klussmann, S. et al. (2009). The death receptor CD95 activates adult neural stem cells for working memory formation and brain repair. Cell Stem Cell 5, 178-190.

Lowenstein, P. R. and Castro, M. G. (2003). Inflammation and adaptive immune responses to adenoviral vectors injected into the brain: peculiarities, mechanisms, and consequences. Gene Ther. 10, 946-954.

Mori, T., Tanaka, K., Buffo, A., Wurst, W., Ku□hn, R. and Go□tz, M. (2006). Inducible gene deletion in astroglia and radial glia–a valuable tool for functional and lineage analysis. Glia 54, 21-34.

Pastrana, E., Cheng, L.-C. and Doetsch, F. (2009). Simultaneous prospective purification of adult subventricular zone neural stem cells and their progeny. Proc. Natl. Acad. Sci. USA 106, 6387-6392.

Srinivas, S., Watanabe, T., Lin, C.-S., William, C. M., Tanabe, Y., Jessell, T. M. and Costantini, F. (2001). Cre reporter strains produced by targeted insertion of EYFP and ECFP into the ROSA26 locus. BMC Dev. Biol. 1, 4.